Supplementary Information

Structural analysis of the yeast Dhh1-Pat1 complex reveals how Dhh1 engages Pat1, Edc3 and RNA in mutually exclusive interactions

Humayun Sharif[1], Sevim Ozgur[1], Kundan Sharma[2], Claire Basquin[1], Henning Urlaub[2] and Elena Conti[1]*

[1]Structural Cell Biology Department, Max Planck Institute of Biochemistry, Munich, D-82152 Germany

[2]Max Planck Institute of Biophysical Chemistry, Am Faßberg 11, 37077 Göttingen, Germany

Supplementary Figures

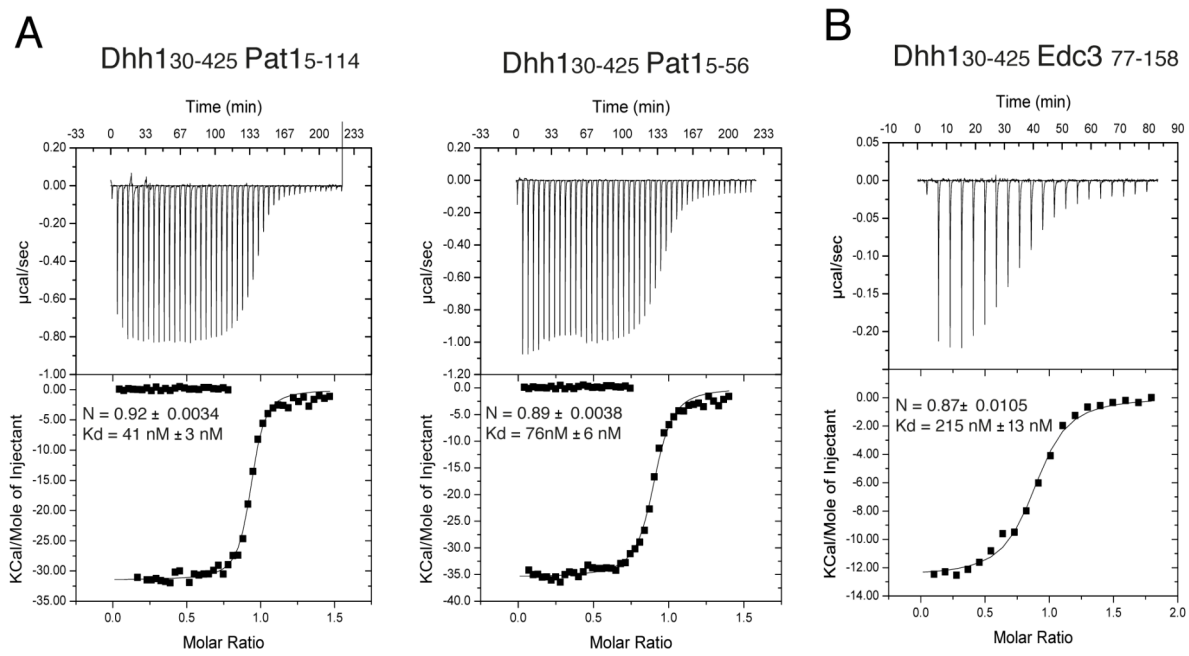

Figure S1

Quantitative analysis of yeast Dhh1-Pat1 and Dhh1-Edc3 interaction

(**A**) Isothermal titration calorimetry (ITC) of $Dhh1_{30-425}$ with His-SUMO-$Pat1_{5-56}$ and $Pat1_{5-114}$. Experiments were performed as described for Figure 1D.

(**B**) ITC of $Dhh1_{30-425}$ with His-SUMO-$Edc3_{77-158}$. Experiments were performed as described for Figure 1D.

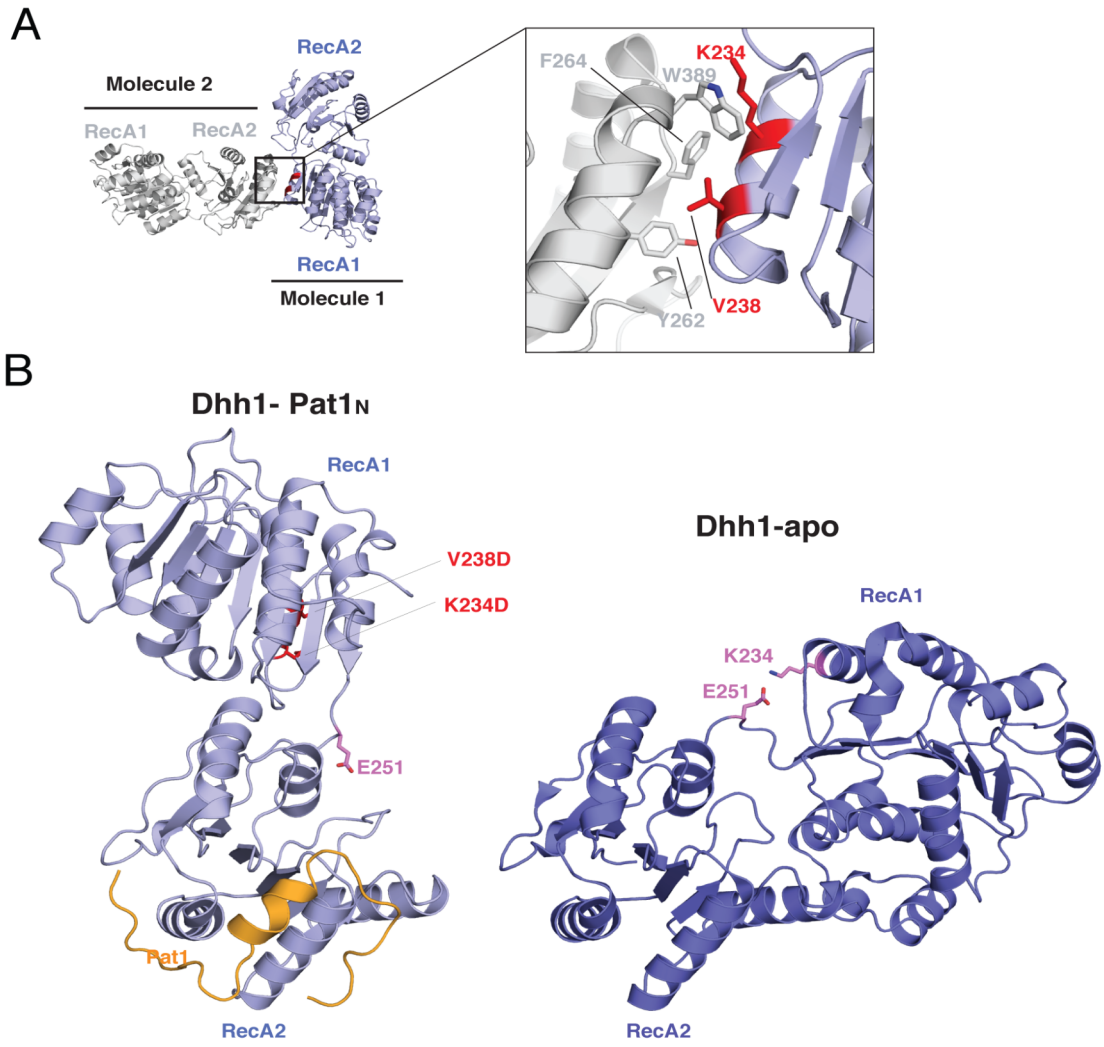

Figure S2

Intermolecular and intramolecular Dhh1 interactions in the crystals

(**A**) The close-up view shows the crystal lattice contacts of yeast Dhh1 wild-type crystals (45). The RecA2 domain of one Dhh1 molecule (in blue) interacts with the RecA1 domain of a neighbouring one (in gray), at the so-called FDF-binding site (patch1). The residues of RecA1 mutated for crystallization of the yeast Dhh1-Pat1 and Dhh1-Edc3 complexes are highlighted in red.

(**B**) The crystal structure of wild-type Dhh1 in the unbound state (45) is shown on the right, in the same orientation as the structure of the yeast Dhh1 K234D, V238D mutant in complex with Pat1 (on the left) after superposition of the RecA2 domains. On the right, the intramolecular interaction of K234 (on

RecA1) and E251 (on RecA2) is highlighted. This interaction is impaired in the mutant we have used for crystallizing the complexes.

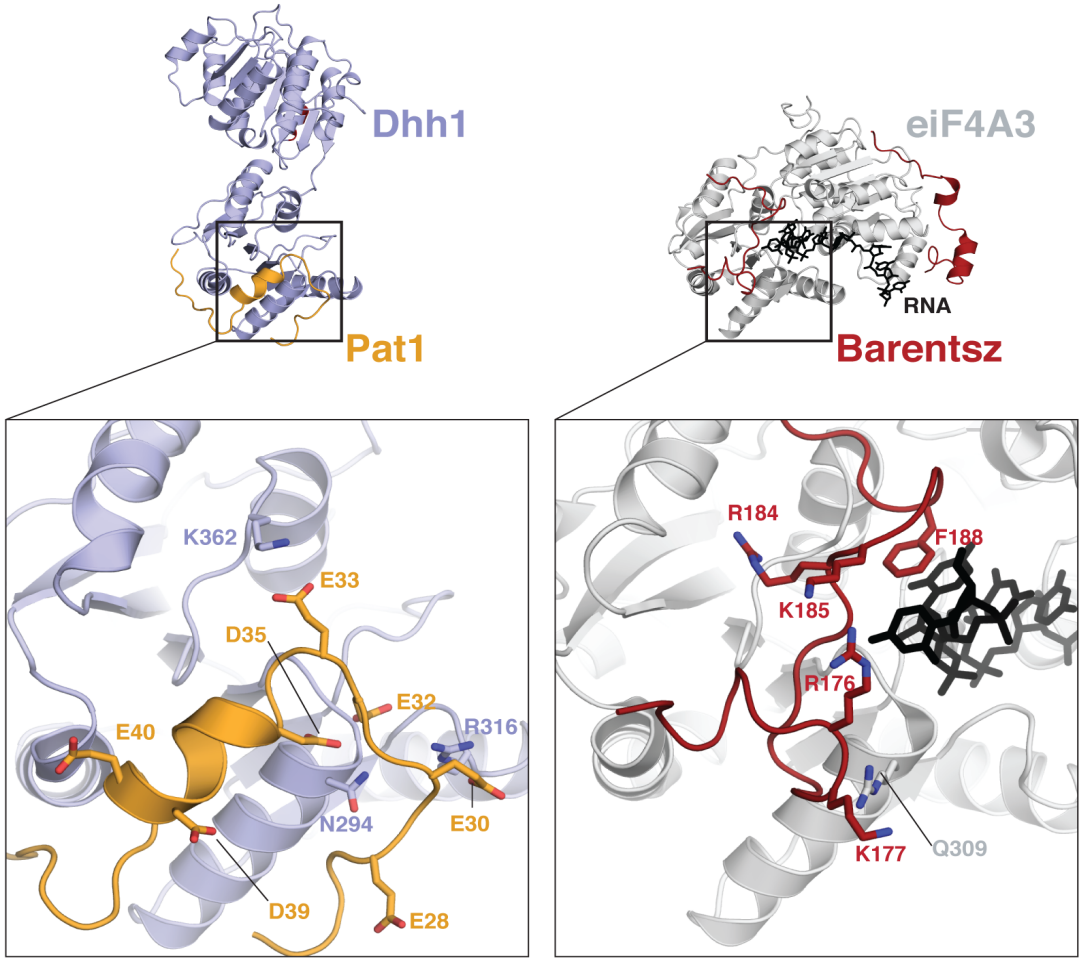

Figure S3

Different DEAD-box proteins use the patch 3 surface to bind regulators

Close-up views of the negatively-charged residues of yeast Pat1 lining the patch 3 surface of Dhh1 (left panel). The right panel shows the structure of human eIF4AIII (gray), Btz (red) and RNA (in black) extracted from the structure of the EJC (54, 55) and viewed in the same orientation as the structure in the left panel, after superposition of the RecA2 domains. Positively-charged residues of Btz line the corresponding patch 3 surface of eIF4AIII and approach the RNA-binding site.

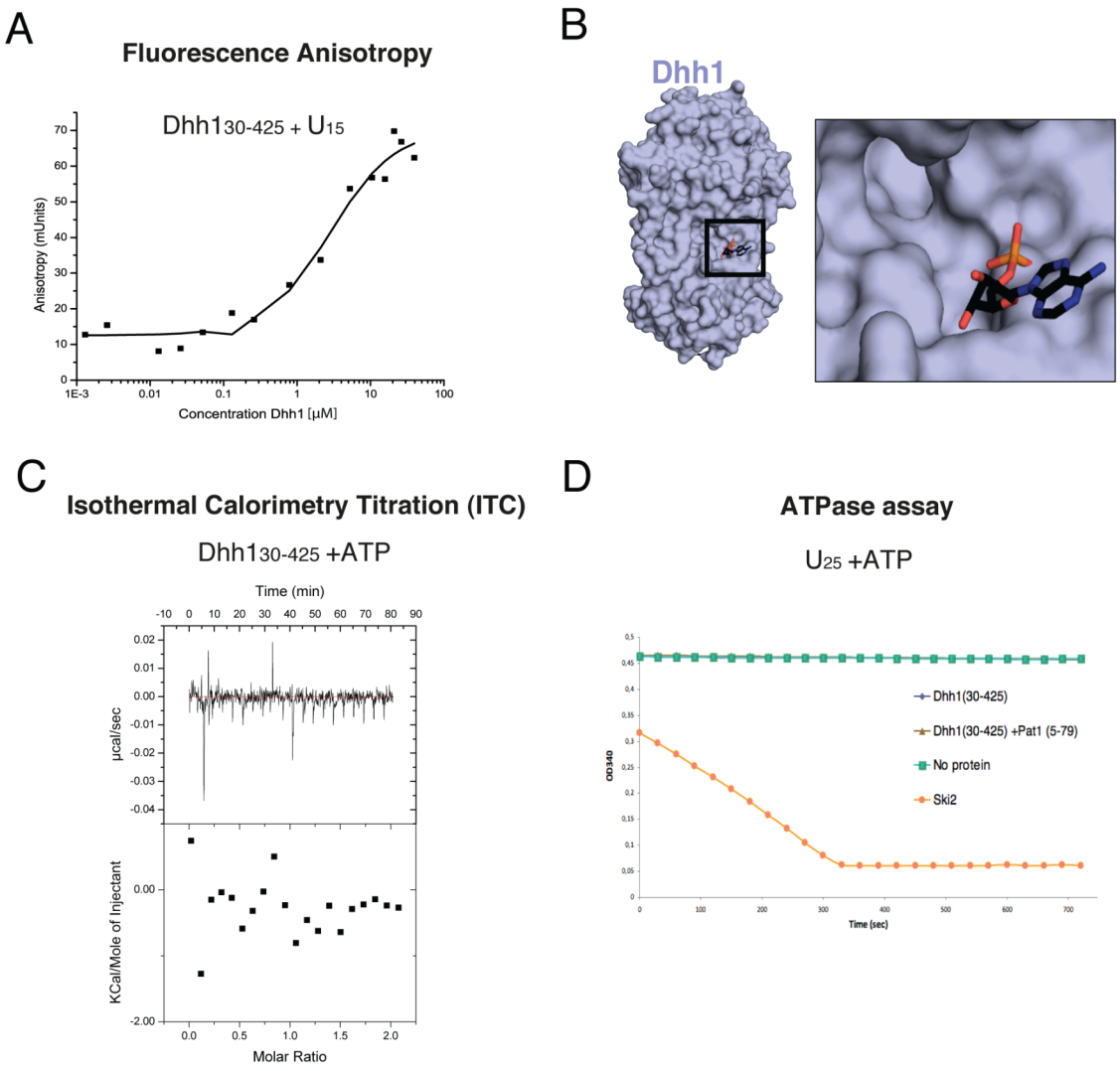

Supplementary Figure S4

RNA-binding and nucleotide-binding properties of the Dhh1 DEAD-box core

(**A**) Quantitative analysis of $Dhh1_{30-425}$ binding to a U_{15} RNA by fluorescence anisotropy (FA). FA measurements were performed with a 5'-6-carboxy-fluorescein (6-FAM)-labeled U_{15} RNA at 20°C on a Genios Pro (Tecan) using 50µl-reactions. The RNA was dissolved to a concentration of 9.6 nM and incubated with $Dhh1_{30-425}$ at different concentrations in 25mM MOPS pH 7.0, 150 mM NaCl, 10mM MgCl2 and 2mM β-mercaptoethanol. The excitation and emission wavelengths were 485nm and 535 nm, respectively. Each titration point was measured three times using ten reads with an integration time of 40 µs. The data were analyzed using nonlinear regression fitting using the Origin software.

(**B**) Surface representation of apo Dhh1 with an ATP analogue modeled from the Dbp5-AMPPNP-RNA structure (60) after superposition of the RecA2 domains. Only the α-phosphate of ATP (in red) is in principle accessible in this closed conformation of Dhh1.

(**C**) ITC of $Dhh1_{30-425}$ with ATP. Experiments were performed as described as for Figure 1D.

(**D**) ATPase assays performed in the presence of a U_{25} RNA with $Dhh1_{30-425}$ either alone (blue diamonds) or in complex with $Pat1_{5-79}$ (brown triangles). The activity of Ski2 (61) is shown as a control (orange circles). The data represent mean values and standard deviations from three independent experiments. The measurements were carried out as reported in (61).

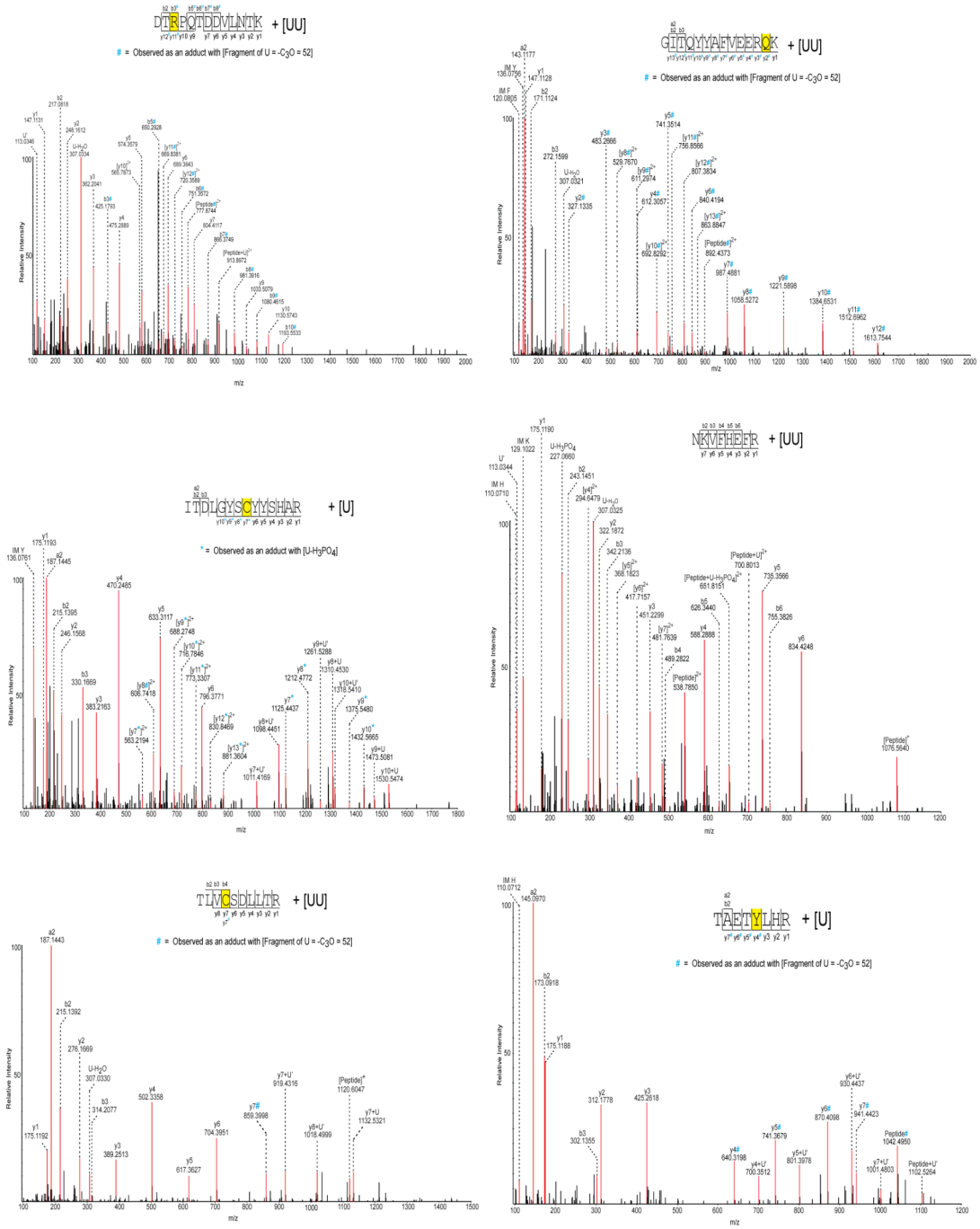

Figure S5

Dhh1-RNA crosslinking and mass spectrometry analysis

MS/MS spectra of Dhh1 peptides with an additional mass that corresponds to uracil nucleotides. Peptide sequence and the fragment ions are indicated on the top. The crosslinked residues are

highlighted in yellow. The peptide fragmentation occurs with the cleavage of amide bonds resulting in b-ions and y-ions when the charge is retained by the amino-terminal and carboxy-terminal fragments, respectively. Asterisk (*) and hash (#) indicate the ions that were observed with a mass shift corresponding to U-H_3PO_4 and $–C_3O$ (a 52 Da fragment of Uracil), respectively. IM: Immonium ions. U': U marker ion of 113.03 Da.

Supplementary Methods

UV induced Protein-RNA crosslinking and enrichment of cross-linked peptides

UV cross-linking and enrichment of cross-linked peptides was performed according to the established protocols described in (62). Briefly, 1 nmol of the single stranded U_{15} RNA oligonucleotide and 1 nmole of $Dhh1_{30-425}$ were mixed in a 1:1 molar ratio and the total reaction volume was made up to 100 µl in 20 mM HEPES pH 7.5, 50 mM NaCl, 2 mM DTT and 5 mM EDTA. The mixture was incubated on ice overnight. The samples were then transferred to black polypropylene microplates (Greiner Bio-One) and irradiated at 254 nm for 10 minutes. After ethanol precipitation the samples were denatured in 4M Urea, 50 mM Tris-HCl pH 7.9 and digested for 2 hours at 52°C with 1 µg RNase A (Ambion, Applied Biosystems). Following RNA digestion, proteolysis with trypsin (Promega) was performed overnight at 37°C. The sample was desalted on an in-house prepared C18 (Dr. Maisch GmbH) column and the cross-linked peptides were enriched on an in-house prepared TiO_2 (GL Sciences) column using the protocol described in (62). The samples were dried and then resuspended in 10 µl sample solvent (5% v/v ACN, 1% v/v FA) for mass spectrometry analysis.

Nano-liquid chromatography and MS analysis

5 µL of the above sample was injected onto a nano-liquid chromatography system (Agilent 1100 series, Agilent Technologies) including a C18 trapping column of length ~2 cm and inner diameter 150 µm, in-line with a C18 analytical column of length ~15 cm and inner diameter 75 µm (both packed in-house, C18 AQ 120 Å 5 µm, Dr. Maisch GmbH). Analytes were loaded on the trapping column at a flow rate of 10 µL/min in buffer A (0.1% v/v FA) and subsequently eluted and separated on the analytical column with a gradient of 7–38% buffer B (95% v/v acetonitrile, 0.1% v/v FA) with an elution time of 33 min (0.87%/min) and a flow rate of 300 nL/min. Online ESI-MS was performed with an LTQ-Orbitrap Velos instrument (Thermo Scientific), operated in data-dependent mode using a TOP10 method. MS scans were recorded in the m/z range of 350-1600 and for subsequent MS/MS top 10 most intense ions were selected. Both Precursor ions as well as fragment ions were scanned in the Orbitrap. Fragment ions were generated by HCD activation (higher energy collision dissociation, normalized collision energy=40), and recorded from m/z=100. As precursor ions as well as fragment

ions were scanned in the Orbitrap, the resulting spectra were measured with high accuracy (< 5 ppm) both in the MS and MSMS level.

Data analysis

The MS .raw files were converted into the .mzML format with msconvert (63). Protein-RNA cross-links were analyzed using OpenMS (64, 65) and OMSSA (66) as search engine. Data analysis workflows were assembled based on (66). The high scoring cross-linked peptides were manually annotated for confirmation. Protein RNA interactions between the N1T25LP complex and polyU RNA was analyzed with UV induced protein-RNA crosslinking followed by mass spectrometry. Seven peptides of Dhh1 protein were observed carrying an additional mass corresponding to Uracil nucleotides.

Supplementary References

45. Cheng,Z., Coller,J., Parker,R. and Song,H. (2005) Crystal structure and functional analysis of DEAD-box protein Dhh1p. *RNA*, **11**, 1258–1270.

54. Bono,F., Ebert,J., Lorentzen,E. and Conti,E. (2006) The crystal structure of the exon junction complex reveals how it maintains a stable grip on mRNA. *Cell*, **126**, 713–725.

55. Andersen,C.B.F., Ballut,L., Johansen,J.S., Chamieh,H., Nielsen,K.H., Oliveira,C.L.P., Pedersen,J.S., Seraphin,B., Le Hir,H. and Andersen,G.R. (2006) Structure of the exon junction core complex with a trapped DEAD-box ATPase bound to RNA. *Science*, **313**, 1968–1972.

60. Moeller,von,H., Basquin,C. and Conti,E. (2009) The mRNA export protein DBP5 binds RNA and the cytoplasmic nucleoporin NUP214 in a mutually exclusive manner. *Nat Struct Mol Biol*, **16**, 247-254.

61. Halbach,F., Rode,M. and Conti,E. (2012) The crystal structure of S. cerevisiae Ski2, a DExH helicase associated with the cytoplasmic functions of the exosome. *RNA*, **18**, 124–134.

62. Kramer,K., Hummel,P., Hsiao,H., Luo,X., Wahl,M. and Urlaub,H. (2011) Mass-spectrometric analysis of proteins cross-linked to 4-thio-uracil- and 5-bromo-uracil-substituted RNA. *Int J Mass Spectrometry*, **304**, 184–194.

63. Kessner, D., Chambers, M., Burke, R., Agus, D. & Mallick, P. (2008) ProteoWizard: open source software for rapid proteomics tools development. *Bioinformatics* **24**, 2534–2536.

64. Sturm,M., Bertsch,A., Gropl,C., Hidebrandt,A., Hussong,R., Lange,E., Pfeifer,N., Shulz-Trieglaff,O., Zerck,A., Reinert,K. and Kohlbacher O. (2011) . OpenMS - an open-source software framework for mass spectrometry. *BMC Bioinformatics* **9**, 163.

65. Bertsch,A., Gröpl,C., Reinert,K. and Kohlbacher,O. OpenMS and TOPP: open source software for LC-MS data analysis. *Methods Mol Biol* **696**, 353–367 (2011).

66. Geer, L.Y., Merkey,S.P., Kowalak, J.A., Wagner,L, Xu,M., Maynard,D.M., Yang,X., Shi,W. and

Bryant,S.H. (2004) Open mass spectrometry search algorithm. *J Proteome Res* **3**, 958–964.